Residual stresses in ss316l specimens after deposition of melted filler wire

Sébastien Rouquette, Camille Cambon, Issam Bendaoud, Fabien Soulié

RESIDUAL STRESSES IN SS316L SPECIMENS AFTER DEPOSITION OF MELTED FILLER WIRE

S. Rouquette[1] , C. Cambon, I. Bendaoud, F. Soulié

LMGC, Univ. Montpellier, CNRS, Montpellier, France

ABSTRACT

In this communication, two specimens are studied upon which a filler-wire is melted and deposited under electric arc heating. The process of interest is called wire and arc additive manufacturing. Such process produces mechanical parts with high tensile stresses and important geometrical distortions. The focuse is made on the residual stresses in the specimen. The effect of each deposited layer on the residual stresses is investigated with the neutron diffraction technique. The highest longitudinal stress values are measured under and at the parent - deposit surface where occurs the highest heating and cooling phases. The deposition of the 2^{nd} layer has reduced the tensile longitudinal stress values of 60 MPa. The thermal cycle due to the deposition of the 2^{nd} layer likely acted as a partial heat treatment of the previous melted and heat affected zones. A 2D stress map has been done from the one layer specimen lots of nuetron diffraction have been done. This 2D stress map shows that the inner part of the specimen is under compressive stress while the deposits are under tensile stress with a stress peak located near the parent - deposit interface. The longitudinal stress decreased from this peak till the top surface of the last deposit.

Keywords: WAAM, GMAW, Neutron Diffraction, Residual stresses

1 Introduction

Additive manufacturing (AM) techniques are based on layer-by-layer accumulation of molten material with the aid of CAD model in the aim to develop three dimensional parts [1]. Compared with traditional manufacturing, Additive Manufacturing (AM) have the ability to produce complex components with less waste of materials and energy [1, 2, 3]. Metal additive manufacturing processes utilize laser beam, electron beam, or electric arc as the heat source and the feedstock material can be in the form of powder, wire, or sheet [1]. The processes using electric arc energy are named wire arc additive manufacturing (WAAM). This technique has the potential to build up parts up to few meters with relatively low forming costs and high manufacturing efficiencies [4]. In the WAAM process, the metallic wire is heated by the electric arc, then melted and transferred to the melt pool. As the welding torch moves on, the rear of the weld pool solidifies letting place to a deposit. Thus another layer is deposited on the top of the former. The AM part is built layer-by-layer.

However, few issues slow the wide spread of WAAM techniques such as : large surface roughness, anisotropy of the microstructure, high hardness, ... As the number of layers increases, the microstructure exhibits large columnar grains up to millimetre size crossing the layers. Furthermore, high tensile residual stresses and important distortions are present in WAAM parts [5]. In welded structures, the tensile residual stresses reduce the fatigue strength and the toughness [6]. Residual stresses are mainly caused by the compressive yielding that occurs around the melted zone as the material heats and expands under arc heating. When the weld metal cools down, it shrinks which causes a tensile residual stresses, particularly in the longitudinal direction.

Two specimens are studied in this communication: the first one has one deposit and the second one has two overlaid deposits (or layers) on parent's edge. The parent material is in SS304L and the filler wire is in stainless steel 316L. A Cold Metal Transfer Gas Metal Arc Welding generator (CMT-GMAW) was used to melt the filler wire and, then, it is dropped off on the parent material. The experimental setup has been designed such as the AM parts are built under plane stress assumption.

[1]corresponding author: sebastien.rouquette@umontpellier.fr

As a consequence, the strain - stress analysis is reduced to two dimensions. Neutron diffraction (ND) strain measurement has been used to evaluate the residual stress field in the two specimens. ND is a non-destructive technique that provides insights into strain and stress fields deeper inside the engineering structures [7]. The neutron diffraction measurement have been performed at the SALSA beam line, ILL, Grenoble, France [8, 9]. The residual stress distribution inside the parent material and the deposits are presented and the influence of the deposition of 2^{nd} layer is discussed especially in the critical melted zone where the high stress gradient and textured microstructure are presents.

2 Description of the specimens

2.1 Operating conditions and specimen geometry

A schematic representation of the specimen with 1 layer is reported in figure 1 and a photography of the two layers specimen is presented in figure 2. The parent material is made of stainless steel 304L and the dimensions are 149 x 100/53 x 6 mm^3 . During the deposition procedure, the parent material is clamped on the left side (the largest). The other extremity is free to move. Up to 2 layers are deposited on the top surface of the parent as depicted in figure 1. The neutron strain scans were performed along 3 different sections for the 1 layer specimen in the aim to get a full 2D residual stress field while it has been done along one line for the second specimen.

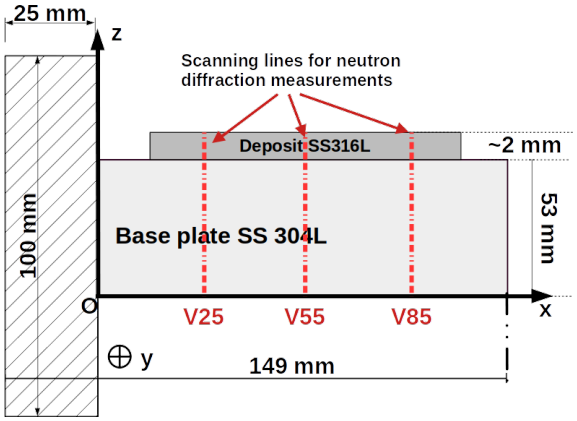

Figure 1: Geometry of the specimen with 1 deposited layer on its thickness and scanning lines used for neutron diffraction.

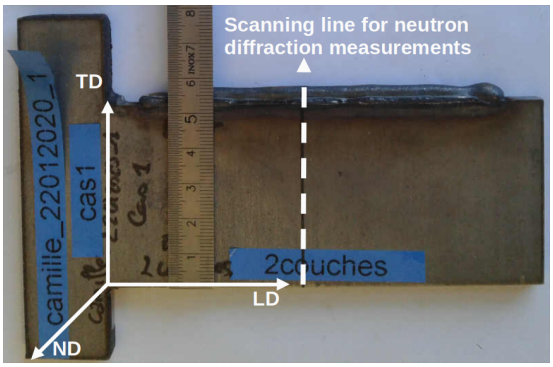

Figure 2: Specimen with two layers. The white dash dotted lines was the only line used for neutron diffraction measurements.

The process parameters: voltage, current, welding speed and shielding gas are reported in table 1. The first layer has been done with an higher energetic parameter in order to reduce the sink effect of the parent material. Then the second layer has been performed with a lower linear welding energy. The parents were cut off with plasma cutting machine from the same SS304L sheet.

parameter	U (V)	I (A)	V (mm/s)	Ws (m/mn)
1st layer	13.4	123	7	4.2
2n layer	13.3	110	7	3.3

Table 1: process parameters used for deposition of the layers. The shielding gas used was a mixture of 98 % Argon with 2% Carbon Dioxyde (CO_2) at flow rate of 15 L/min.

2.2 Texture analysis

The texture analysis has been investigated by electron back scattered diffraction (EBSD) in order

to determine if there was any preferred orientation in the microstructure of either the parent or deposits materials. The studied samples are displayed in figures 3 and 4 extracted at section V55 for both specimen (see figures 1 and 2.

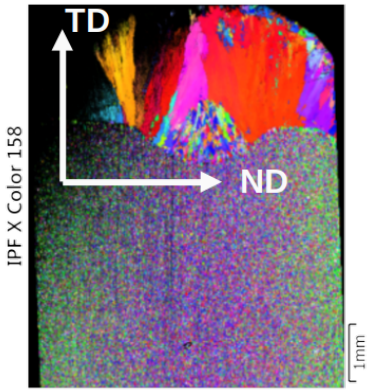

Figure 3: principal direction of grains in the five layers specimen (TD is the transverse direction and ND normal direction). Investigated specimen labelled 21_11_19.

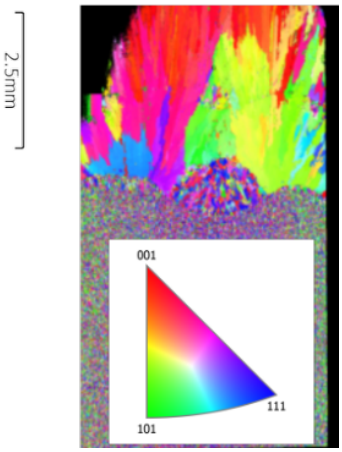

Figure 4: principal direction of grains in the five layers specimen (TD is the transverse direction and ND normal direction). Investigated specimen labelled 21_11_19.

The two figures 3 and 4 exhibit large columnar grains in the direction of deposition (z direction as in figure 1). The length of the grains is of few millimetre for the 2 layers specimen. Unfortunately, the two EBSD figures are of poor quality because the polishing was extremely difficult on the 304L and 316L stainless steels. A small zone of equiaxed grains is visible in the centre of the first layer, see figure 3. The principal cristal direction is 001 as it is observed on the two EBDS figures (red colour). The growth of the grains is characteristic of the WAAM process leading to anisotropic material properties [10]. During the solidification, emergence and growth of dendrites are in the opposite direction to the heat flow. WAAM metallic parts often results in a columnar grain structure, leading to a highly textured material with anisotropic material properties [10].

3 Neutron strain measurements and residual stresses

Neutron diffraction measurements were carried out on SALSA beam line (Strain Analyser for Large and Small scale engineering Applications). SALSA is the dedicated engineering diffractometer Institute Max Von Laue Paul Langevin, Grenoble (France) [11].

A full diffraction pattern was measured at a fixed wavelength, λ = 1.66 Å and a 2θ = 98.502° for Fe-311 cristal plane. Measurements were made along three directions; the longitudinal direction (LD) parallel to the layer, the transverse direction perpendicular to the layer (TD) and the normal direction (ND), perpendicular to the surface of the plate. The normal and longitudinal directions were measured without unmounting the specimen but it required a rotation of the platform. The sample had to be repositioned once to measure the third direction: the transverse one. Instrument gauge volume of 2 x 2 x 0.6 mm^3 was used for measurements in the three directions.

3.1 Theoritical background: from Bragg's law to the stresses

The measurement of residual strains by neutron diffraction is based on Bragg's law [12]:

$$\lambda = 2d_{hkl} \sin \theta_{hkl} \tag{1}$$

where λ is the wavelength of the neutron beam, d_{hkl} is the lattice spacing of atomic planes characterised by Miller indices h k l and $2\theta_{hkl}$ is the scattering angle of the peak being measured. For monochromatic beam diffraction, the wavelength is fixed and its magnitude known and the measurement of $2\theta_{hkl}$ gives the lattice spacing. The strain in the same direction is then computed from the change in the interplanar spacing of the material according to the unstressed state as [13, 14] :

$$\epsilon_i = \frac{d_i - d^0_{hkl}}{d^0_{hkl}} = \frac{sin\theta_i}{sin\theta^0_{hkl}} - 1 \tag{2}$$

It is common use to define that the principal axes for linear welds are the longitudinal direction in the weld (LD), the transverse direction (TD) and the parent material normal direction (ND) [15]. As the parent material thickness is 6 mm and this dimensions is smaller according to the length and heigh, it is assumed that the normal stress will be close to zero. Moreover, it was supposed that LD, TD and ND were the principal directions. Then, the measurements of diffracted 2θ angles were performed in these three directions. Once the three principal strain components are measured, the stress in each direction is calculated using Hooke's law through the following equation:

$$\sigma_{ii} = \frac{E}{1+\nu}\epsilon_{ii} + \frac{\nu E}{(1+\nu)(1-2\nu)}\sum_{i=1}^{3}\epsilon_{ii} \tag{3}$$

where E is the elastic modulus and ν is Poisson's ratio. Crystallographic moduli relevant to the considered single planes (i.e. Fe-311) are required for monochromatic instruments. The macroscopic and crystallographic values of E and ν used in this study were: E = 182 GPa, ν = 0.307. They were sourced from H.M. Ledbetter [16].

The reference θ_0 angle is determined according to the plane stress assumption [17]. The reference θ_0 angle is required for the computation of the strains according equation 2. Thus, it imposes that the normal stress is null: σ_{norm} = σ_{YY} = 0. This condition can be written as follows:

$$\sigma_{YY} = \frac{E}{1+\nu}\epsilon_{YY} + \frac{\nu E}{(1+\nu)(1-2\nu)}(\epsilon_{XX} + \epsilon_{YY} + \epsilon_{ZZ}) \tag{4}$$

It comes for ϵ_{YY}

$$\epsilon_{YY} = \frac{-\nu}{1-\nu}(\epsilon_{XX} + \epsilon_{ZZ}) \tag{5}$$

Secondly, the equation 2 can be simplified such as:

$$\epsilon_{YY} = \frac{\theta_Y - \theta_0}{\theta_0} \tag{6}$$

Finally, by introducing equation 6 into equation 5 and solving for getting θ_0, it comes:

$$\theta_0 \simeq \frac{1-\nu}{1+\nu}[\theta_Y + \frac{\nu}{(1-2\nu)}(\theta_X + \theta_Y + \theta_Z)] \tag{7}$$

Once the longitudinal and transverse strains are calculated, the residuals stresses can be deduced by applying Hooke's law, equation 3. The longitudinal and transverse stresses are opresented in the next section without presenting the micro-strains.

3.2 Residual stress field in the one layer specimen

The specimen was scanned with neutrons along 3 different lines: 3 verticals as presented in figure 1. The three longitudinal stress distributions are reported in figure 5. The three longitudinal stress distributions are very similar in the parent material. The few differences are noticed close to and

within the melted zone thus in the deposit for z $>$ 45 mm. The longitudinal stresses in sections V25 and V85 are also very similar in the melted zone. The one calculated in section V55 shows higher longitudinal stresses. The maximum longitudinal stress, 234$\pm$7.7 MPa is reached at z = 50 mm for section V55. For sections V25 and V85, the maximum stress values are respectively 205$\pm$5.2 MPa at z = 50 mm and 218.7$\pm$5.3 MPa at z = 51 mm. No stress data are available in the middle of the deposit (z $\simeq$ 54 mm). The one measured at z = 53 mm is in the parent's melted zone.

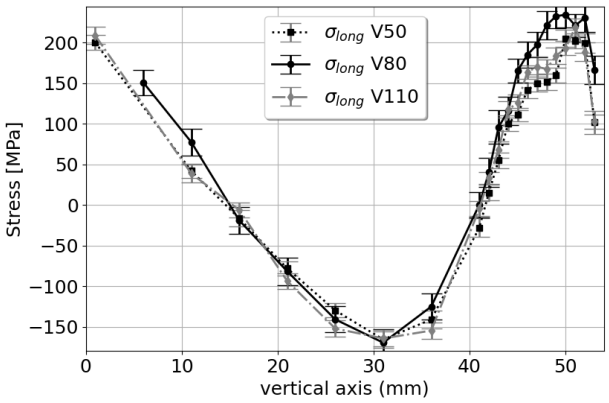

Figure 5: longitundinal stress for L1 at the three sections.

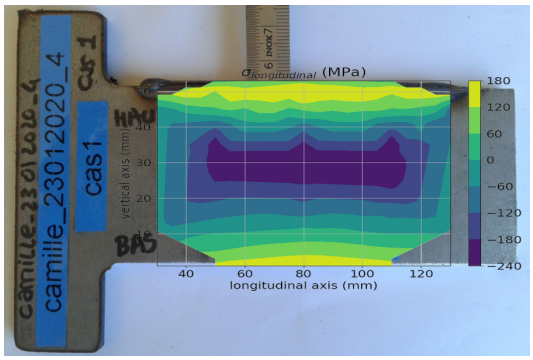

Figure 6: 2D longitudinal stress field within the one layer specimen.

The three longitudinal stresses have the same evolution from the bottom of the parent to the top of the deposit (thus top parent). At the bottom of the parent material, the longitudinal stress values are tensile with a maximum value of 200 Mpa at z = 1 mm. Then the longitudinal stress decreases quickly to a minimum of -169 MPa at z = 31 mm. Afterwards, the stress increases until the parent / deposit interface with values reaching 218 to 234 MPa at z = 50 mm, see 2. A large zone inside the parent (15 mm to 41 mm) is under compressive stress. The highest longitudinal stress values at the parent / deposit interface are inherent to the arc welding process. Coules et al investigated the in-situ plastic strain generation during a GTAW experiment[18]. They noticed that the material developed plastic strain around the melted zone. This zone was subjected to high heating what produced high thermal gradient through the parent from its top to its inside. This strong thermal gradient produced a thermal compression of material inside of it during the heating time. During the cooling, the melted zone solidified which in turn generated a shrinkage of the melted pool zone so tensile stress while within the unmelted zone of the parent was subjected to compressive stress.

vertical position	1 mm	11 mm	21 mm	31 mm	41 mm	46 mm	51 mm	53 mm
V25	200 $\pm$ 4.5	41.8 $\pm$ 4.3	-78.3 $\pm$ 4.5	-165.7 $\pm$ 5	-28.2 $\pm$ 5.7	141.2 $\pm$ 4.8	201.8 $\pm$ 4.4	101.6 $\pm$ 6.9
V55	-	77.3 $\pm$ 8.2	-81.8 $\pm$ 8.3	-169.7 $\pm$ 8.3	0.2 $\pm$ 7.7	184.8 $\pm$ 8	220.7 $\pm$ 7.1	166.2 $\pm$ 8.7
V85	208.8 $\pm$ 5.4	38.6 $\pm$ 5.4	-93.8 $\pm$ 4.7	-164.4 $\pm$ 5	-4.8 $\pm$ 4.5	163.4 $\pm$ 4.1	218.7 $\pm$ 5.3	102.4 $\pm$ 4.4

Table 2: Longitudinal stress values along the vertical axis for the three sections.

A 2D field of the longitudinal stresses is displayed in figure 6. All scanned lines with some extra points added to a interpolation function allowed to plot this field within the 1 layer specimen. The compressive zone is clearly visible inside the parent and represents a wide part of the parent. The longitudinal stress peaks are located at the parent / deposit interface as already mentioned. The bottom part of the specimen experiences tensile stress. It is supposed to be a result of a stress balance within the specimen.

3.3 Comparison of residual stress distributions in both specimens

The 2^{nd} layer was deposited such that the end of the previous layer was its starting point. A

cooling time of 35 s was also applied before starting the 2^{nd} deposit. Indeed, this cooling was not enough for the specimen to get back to the ambient temperature.

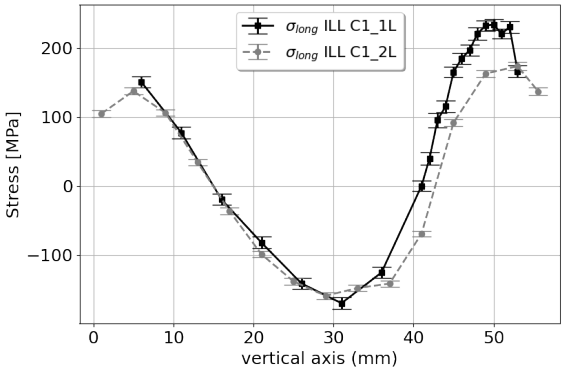

Figure 7: Longitudinal stress L1 vs L2 at section V55.

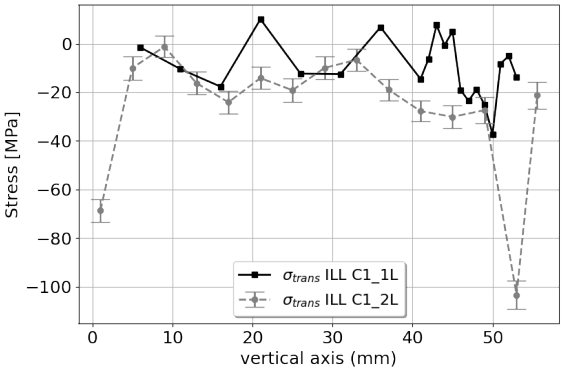

Figure 8: Transverse stress L1 vs L2 at section V55.

The comparison of longitudinal stresses is given in figure 7. The two longitudinal stress distributions are similar in the half bottom of the parent (z $<$ 31 mm) even if the tensile stress reached at the bottom (z = 1 mm) is lower after 2 deposits with a value of 104.8 $\pm$ 4.6 MPa as reported in table 3. In the top half part of the specimen, the longitudinal stress distributions follow the same trend but the values of the 2 layers specimen are lower. The highest stress value is 173 MPa reached at z = 53 mm so 2 mm under the interface between the 1^{st} and 2^{nd} layers. This value is about 60 MPa lower than the one measured for the 1 layer specimen at z = 50 mm (3 mm under the interface parent / deposit). The longitudinal stresses decreases slowly to the top deposit surface as a value of 137.3 $\pm$ 5.4 MPa is measured at 55 mm (the top surface of the deposit is near z = 57 mm).

vertical position	1 mm	11 mm / 13 mm	21 mm	31 mm / 33 mm
1 layer specimen (MPa)	-	77.3 $\pm$ 8.2	-81.8 $\pm$ 8.3	-169.7 $\pm$ 8.3
2 layers specimen (MPa)	104.8 $\pm$ 4.6	34.7 $\pm$ 4.6	-98.8 $\pm$ 4.5	-147.8 $\pm$ 4.6

vertical position	41 mm	46 mm / 45 mm	51 mm	53 mm	55 mm
1 layer specimen (MPa)	184.8 $\pm$ 8	220.7 $\pm$ 7.1	166.2 $\pm$ 8.7	-	
2 layers specimen (MPa)	-68.9 $\pm$ 4.2	91.9 $\pm$ 4.7	-	-173.7 $\pm$ 5.7	137.3 $\pm$ 5.4

Table 3: Comparison of longitudinal stresses for 1 layer and 2 layers speciments at section V55. The reference $2\theta_0$ angle was calculated according the plane stress assumption.

The two transverse stress distributions are presented in figure 8. These distributions are very similar from the parent's bottom to the deposits's top. As the plane stress assumption used for estimating the reference $2\theta_0$ angle imposed that σ_{norm} = σ_{YY} = 0 and the transverse stress values are almost constant and close to zero, the mechanical loading, at section V55, is almost uni-axial.

4 Discussion: effect of the 2^{nd} layer deposition on residual stresses

The deposition of the 2^{nd} layer had led to a decrease of the maximum longitudinal stress values without modifying the minimum one. The decrease of tensile longitudinal stresses is significant: up to 60 MPa in the melted zone and up to 100 MPa at the parent's bottom. The 2^{nd} layer was deposited 35 s after the previous one was finished and its starting point was where the previous one ended up. The specimen did not get enough time to reach the initial temperature so the 2^{nd} layer was deposited

on a warmer specimen, especially on a warmer surface. The temperature was monitored with a K-type thermocouple of 0.5 mm diameter located in section V55, 3 mm below the parent top surface. At the beginning of the 2^{nd} layer, the recorded temperature was close to 300°C while the initial parent temperature before the deposition of the 1^{st} deposit was close to 20°C. The second thermal cycle (heating then cooling phases) generated during the deposition of the 2^{nd} layer did not produce a strong material compression during the heating phase. Furthermore, the 2^{nd} layer started where the specimen was the hottest and finished where it was the "coldest". This is probably why there was no change in the compressive zone. The minimum longitudinal stress value did not change significantly nor its position within the parent. The compressive zone inside the parent became a little be larger. It was also observed that the melted pool was longer during the deposition of the 2^{nd} layer. The re-melting of one part of 1^{st} of the deposit led to a reset of the stresses in this zone (the melted pool is often supposed to undergo low stresses). During the solidification, this longer melted zone shrinked again but under different thermal conditions as well. Indeed, the 2^{nd} cooling rate, estimated to 8.4 °C/s, was also lower than the 1^{st} one, estimated to 11.2 °C/s. The lower cooling rate likely acted as heat treatment and produced a slight stress relief nearby the 2^{nd} melted zone. The north american stainless steel recommends stress relief heat treatment for SS316L in the range [570°C - 830°C] up to 60 min. The thermocouple located at z = 50 mm (so 3 mm under the parent's top surface) varied exactly in this temperature range but for a shorter duration (45 s). Real Heat treatment procedure (700°C for 2 hours) of Additive Manufactured SS316L part made with Laser Bead Powder process has reduced the tensile stresses [19]. Despite the shorter duration of this zone, the second thermal deposition cycle has probably decreased the tensile stresses nearby the melted zone what also induced a decrease of tensile stress in the parent's bottom.

5 Conclusion

In this communication, residual stress fields into one layer and two layers specimens have been presented. This work aims to understand the generation of the stresses during wire and arc additive manufacturing especially to understand the effect of the next deposit on the residual stresses resulting of the 1^{st} deposit. The residual stresses were measured with the neutron diffraction technique at the SALSA beamline, Institut Laue Langevin, in Grenoble (France). The neutron diffraction measurements provided valuables data. The one layer specimen has been neutron scanned along few lines what allowed to do a 2D map of the longitudinal and transverse stresses in the specimen. The two layer specimen was only scanned along one line. Then the residual stresses for both specimens were compared along the same line. It appeared that the 2^{nd} thermal cycle occuring during the deposition of the 2^{nd} layer produced a partial stress relief nearby the melted zone. After the 1^{st} deposition of the layer, this zone exhibited high longitudinal tensile stresses up to 234 MPa while the longitudinal stress decreased to 173 MPa after the deposition of 2^{nd} layer. This trend is interesting as it may be used to lower the tensile stresses within an Additive Manufactured part by controlling some process parameters : welding current, voltage and speed and the cooling time between two deposits.

Acknowledgements

The authors wish to acknowledge the scientific support and technical from Sandra CABEZA of the institute Max von Laue – Paul Langelin, SALSA beam line.

References

[1] W. Jin, C. Zhang, S. Jin, Y. Tian, D. Wellmann, and W. Liu. Wire arc additive manufacturing of stainless steels: A review. *Applied Sciences (Switzerland)*, 10(5), 2020.

[2] D. Ding, Z. Pan, D. Cuiuri, and H. Li. A multi-bead overlapping model for robotic wire and arc additive manufacturing (WAAM). *Robotics and Computer-Integrated Manufacturing*, 31:101–110, 2015.

[3] F. Martina, J. Mehnen, S. W. Williams, P. Colegrove, and F. Wang. Investigation of the benefits of plasma deposition for the additive layer manufacture of Ti-6Al-4V. *Journal of Materials Processing Technology*, 212(6):1377–1386, 2012.

[4] L. Li W.U.H. Syed, A. Pinkerton. A comparative study of wire feeding and powder feeding in direct diode laser deposition for rapid prototyping. *Applied Surface Science*, 247:268–276, 2005.

[5] J. Ding, P. Colegrove, J. Mehnen, S. Ganguly, P. M Sequeira Almeida, F. Wang, and S. Williams. Thermo-mechanical analysis of Wire and Arc Additive Layer Manufacturing process on large multi-layer parts. *Computational Materials Science*, 50(12):3315–3322, 2011.

[6] P. Colegrove, C. Ikeagu, A. Thistlethwaite, S. Williams, T. Nagy, W. Suder, A. Steuwer, and T. Pirling. Welding process impact on residual stress and distortion. *Science and Technology of Welding and Joining*, 14(8):717–725, 2009.

[7] W. Allen, C. Andreani, M.T. Hutchings, and C.G. Windsor. Neutron diffraction methods for the study of residual stress fields. *Advances in Physics*, 34:445–473, 1985.

[8] S. Rouquette, I. Bendaoud, S. Cabeza, C. Cambon, F. Deschaux-Beaume, C. Hacquard, T. Pirling, and F. Soulié. Strain/stress measurement of 316l stainless steel additively manufactured walls with gas metal arc welding process. *Institut Laue-Langevin (ILL)*, 2020.

[9] S. Rouquette, I. Bendaoud, S. Cabeza, C. Cambon, and F. Soulié. Residual stress state of additive manufactured 316l stainless steel parts: Round 2. *Institut Laue-Langevin (ILL)*, 2021.

[10] S. Pratihar, M. Turski, L. Edwards, and P. J. Bouchard. Neutron diffraction residual stress measurements in a 316L stainless steel bead-on-plate weld specimen. *International Journal of Pressure Vessels and Piping*, 86(1):13–19, 2009.

[11] T. Pirling, G. Bruno, and P. J. Withers. SALSA-A new instrument for strain imaging in engineering materials and components. *Materials Science and Engineering A*, 437(1):139–144, 2006.

[12] M.T. Hutchings, P.J. Withers, T.M. Holden, and T. Lorentzen. *Introduction to the Characterization of Residual Stress by Neutron Diffraction*. Taylor and Francis, 2005.

[13] A. D. Krawitz and R. A. Winholtz. Use of position-dependent stress-free standards for diffraction stress measurements. *Materials Science and Engineering A*, 1994.

[14] C. Ohms, R. C. Wimpory, D. E. Katsareas, and A. G. Youtsos. NET TG1: Residual stress assessment by neutron diffraction and finite element modeling on a single bead weld on a steel plate. *International Journal of Pressure Vessels and Piping*, 86(1):63–72, 2009.

[15] T. M. Holden, H. Suzuki, D. G. Carr, M. I. Ripley, and B. Clausen. Stress measurements in welds: Problem areas. *Materials Science and Engineering A*, 2006.

[16] H. M. Ledbetter. Elastic properties of zinc: A compilation and a review, 1977.

[17] V. Akrivos, R. C. Wimpory, M. Hofmann, B. Stewart, O. Muransky, M. C. Smith, and J. Bouchard. Neutron diffraction measurements of weld residual stresses in three-pass slot weld (Alloy 600/82) and assessment of the measurement uncertainty. *Journal of Applied Crystallography*, 53(5):1–14, 2020.

[18] H.E Coules, P. Colegrove, L.D. Cozzolino, and S.W. Wen. Experimental measurement of biaxial thermal stress fields caused by rc welding. *Journal of Material Processing Technology*, 212:962–968, 2012.

[19] R. J. Williams, F. Vecchiato, J. Kelleher, M. R. Wenman, P. A. Hooper, and C. M. Davies. Effects of Heat Treatment on Residual Stresses in the Laser Powder Bed Fusion of 316L Stainless Steel: Finite Element Predictions and Neutron Diffraction Measurements. *Journal of Manufacturing Processes*, 57:641–653, 2020.